INTERNATIONAL JOURNAL FOR NUMERICAL METHODS IN FLUIDS, VOL. 6, 497–505 (1986)

ON THE EFFECTS OF IRREGULAR BOUNDARIES IN FINITE DIFFERENCE MODELS

GEIR PEDERSEN

Universitetet i Oslo, Matematisk Institutt, PB 1053—Blindern, Oslo 3, Norway

SUMMARY

Propagation of periodic waves in the vicinity of irregular saw-tooth shaped boundaries in finite difference models is investigated. The reflection of an incoming wave from a single saw-tooth boundary is found to be accompanied by a phase shift. It is shown that any wave mode propagating along such a boundary is trapped and decays in the direction normal to the boundary. A wave propagating along a channel with saw-tooth shaped lateral boundaries is influenced by the trapped waves, which leads to a reduction of the phase velocity. Phase velocities obtained from the present normal mode analysis are compared to velocities in numerical experiments. The agreement is excellent.

KEY WORDS Shallow Water Equations Finite Differences Irregular Boundaries

INTRODUCTION

In numerical models for wave propagation in oceans and lakes, implementation of boundaries of rather complex shape is often necessary. Such boundaries are obviously represented most accurately by finite element techniques or by use of curvilinear co-ordinates. Such methods are expensive and generally more troublesome to apply than standard difference methods with rectangular grids. The latter are thus still widely used. In rectangular grids, boundaries are usually approximated by a series of line segments parallel to the axes, as illustrated in Figure 1(a). The corresponding discretization errors are generally of first order in the grid increments and may often be important and even dominant. In this paper we will describe some effects arising from the presence of such saw-tooth boundaries aligned at 45° to the axes. Contrary to boundaries of more complicated shapes, the effects of these may be simply analysed in terms of wave modes.

Weare[1] investigated the solution of the ADI scheme for a flow in a channel aligned at 45° to the axes, as depicted in Figure 1(b). The flow was released from rest with a constant surface slope in the direction of the channel. He experienced a transverse variation of the surface elevation which he also was able to predict analytically. Mørk[2] studied propagation of single pulses of finite length along the same channel. He performed numerical experiments using the ADI scheme as well as the explicit FB (forward–backward) scheme which is described in the next section. For both schemes he observed a significant decrease in phase velocity for narrow channels.

In the next section we study the reflection of a periodic incoming wave from a saw-tooth boundary and prove the existence of waves trapped to this boundary. In the section after that we predict the velocity decrease reported by Mørk[2] by constructing periodic propagating waves satisfying the boundary conditions at the channel walls. We have only considered the FB scheme but our results will probably apply to most schemes based on the grid in Figure 2.

0271–2091/86/080497–09$05.00

Received 30 October 1985
Revised 16 January 1986

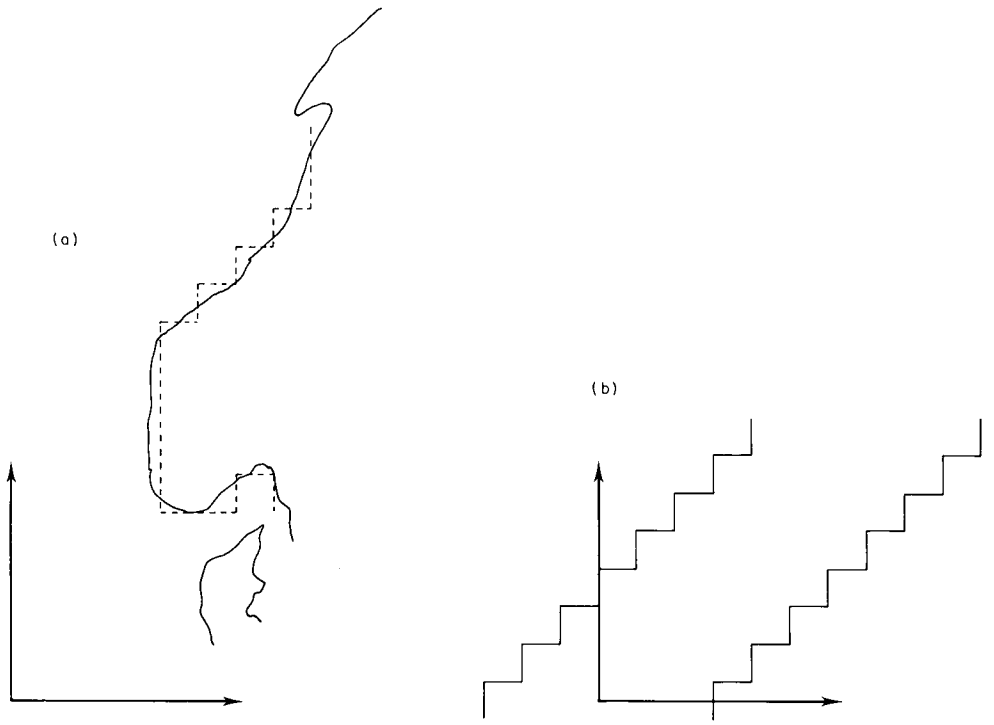

Figure 1. (a) line-segment approximation to an irregular coast; (b) channel aligned 45° to the axes

BASIC EQUATIONS

A Cartesian co-ordinate system with horizontal axes Ox and Oy in the undisturbed free surface is introduced. With the constant depth h as characteristic length scale and $(gh)^{1/2}$ as velocity scale the linear non-dimensional shallow water equation reads

$$\frac{\partial \eta}{\partial t} = -\nabla \cdot \mathbf{v}, \qquad \frac{\partial \mathbf{v}}{\partial t} = -\nabla \eta, \tag{1}$$

where η is the surface elevation, $\mathbf{v} = u\mathbf{i} + v\mathbf{j}$, the horizontal component of the velocity, $\nabla = \mathbf{i}(\partial/\partial x) + \mathbf{j}(\partial/\partial y)$, the horizontal component of the gradient operator, and t is the non-dimensional time. The elimination of $\mathbf{v}$ between the two equations in (1) gives

$$\frac{\partial^2 \eta}{\partial t^2} - \nabla^2 \eta = 0. \tag{2}$$

At a rigid wall we have the zero flux condition:

$$v_n \equiv \mathbf{v} \cdot \mathbf{n} = 0, \tag{3}$$

where $\mathbf{n}$ is the unit normal to the boundary. Using the second equation in (1) we find an alternative form of (3):

$$\frac{\partial \eta}{\partial n} \equiv \mathbf{n} \cdot \nabla \eta = 0. \tag{4}$$

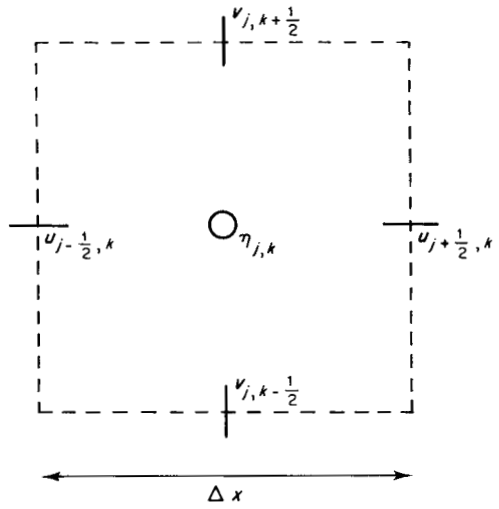

Figure 2. Definition sketch for the grid

Substitution of a plane wave solution $\eta = \hat{\eta} e^{i(\alpha x + \beta y - \omega t)}$ into (2) gives the relation

$$\omega^2 = \alpha^2 + \beta^2. \tag{5}$$

We denote α by $\sigma_1 + i\gamma_1$ and β by $\sigma_2 + i\gamma_2$. A real ω is possible if (i) $\gamma_1 = \sigma_2 = 0$, $|\gamma_2| < |\sigma_1|$, (ii) $\gamma_2 = \sigma_1 = 0$, $|\gamma_1| > |\sigma_2|$, (iii) $\sigma_2 = \kappa\sigma_1$, $\gamma_2 = -\gamma_1/\kappa$ for some real κ. The last alternative corresponds to a wave number vector of the form $\mathbf{k} = \mathbf{k}_1 + i\mathbf{k}_2$ where $\mathbf{k}_1$ and $\mathbf{k}_2$ are real and orthogonal. If $\mathbf{k}_2 = 0$ we have a pure harmonic propagating wave and if $\mathbf{k}_2 \neq 0$ (iii) may be reduced to (i) or (ii) by a rotation of the co-ordinate system. We will be particularly concerned with the case $\alpha = \beta^* = \sigma - i\gamma$, for which (5) gives

$$\omega^2 = \alpha^2 + \alpha^{*2} = 2\sigma^2 - 2\gamma^2 \tag{6}$$

In Figure 2 we have depicted a cell in a standard staggered grid. For simplicity the grid increments Δx and Δy are chosen to be equal throughout this paper. The centre of the cell is located at $(x, y) = (j\Delta x, k\Delta x)$ where we have the η-node. This space discretization is the basis of several numerical schemes.[3] For our investigations we will choose one of the simplest, which we will refer to as the FB (forward–backward) scheme. Our main results will though be valid for most of the differences and are defined correspondingly. Expressed in terms of these operators the FB scheme reads

$$\begin{aligned}
\frac{1}{\Delta t}(u^{n+1}_{j+1/2,k} - u^{n}_{j+1/2,k}) &= -\frac{1}{\Delta x}(\eta^{n}_{j+1,k} - \eta^{n}_{j,k}),\\
\frac{1}{\Delta t}(v^{n+1}_{j,k+1/2} - v^{n}_{j,k+1/2}) &= -\frac{1}{\Delta x}(\eta^{n}_{j,k+1} - \eta^{n}_{j,k}),\\
\frac{1}{\Delta t}(\eta^{n+1}_{j,k} - \eta^{n}_{j,k}) &= -\frac{1}{\Delta x}(u^{n+1}_{j+1/2,k} - u^{n+1}_{j-1/2,k}) - \frac{1}{\Delta x}(v^{n+1}_{j,k+1/2} - v^{n+1}_{j,k-1/2}),
\end{aligned} \tag{7}$$

where n refers to the time $t = n\Delta t$, etc. As in the analytical case, elimination of the velocities gives a second-order equation for η:

$$\frac{1}{\Delta t^2}(\eta^{n+1}_{i,j} - 2\eta^{n}_{i,j} - \eta^{n-1}_{i,j}) = \frac{1}{\Delta x^2}\{(\eta^{n}_{i+1,j} - 2\eta^{n}_{i,j} + \eta^{n}_{i-1,j}) + (\eta^{n}_{i,j+1} - 2\eta^{n}_{i,j} + \eta^{n}_{i,j-1})\}. \tag{8}$$

Substitution of the mode $\eta^n_{j,p} = \hat{\eta} e^{i(\alpha j \Delta x + \beta p \Delta x - \omega n \Delta t)}$ into (8) gives

$$\bar{\omega}^2 = \bar{\alpha}^2 + \bar{\beta}^2, \tag{9}$$

where

$$\bar{\omega} = \frac{2}{\Delta t} \sin \frac{\omega \Delta t}{2}, \quad \bar{\alpha} = \frac{2}{\Delta x} \sin \frac{\alpha \Delta x}{2} \quad \text{and} \quad \bar{\beta} = \frac{2}{\Delta x} \sin \frac{\beta \Delta x}{2}.$$

If α and β are real (9) always gives a real ω provided $\Delta t < 2^{-1/2} \Delta x$. Taylor series expansions in terms of $\alpha \Delta x$, $\beta \Delta x$ and $\omega \Delta t$ lead to

$$\omega^2 = \alpha^2 + \beta^2 + \tfrac{1}{12} \Delta t^2 (\alpha^2 + \beta^2)^2 - \tfrac{1}{12} \Delta x^2 (\alpha^4 + \beta^4) + \ldots \tag{10}$$

For the case $\alpha = \sigma - i\gamma$, $\beta = \sigma + i\gamma$ we obtain

$$\bar{\omega}^2 = 2\bar{\sigma}^2 + 2(1 - \tfrac{1}{2} \Delta x^2 \bar{\sigma}^2)(\overline{i\gamma})^2, \tag{11}$$

where the overbars have the same interpretation as in (9). We note that $(\overline{i\gamma}) = i(2/\Delta x) \sinh(\gamma \Delta x/2)$. Taylor series expansions applied to (11) lead to

$$\omega^2 = 2\sigma^2 - 2\gamma^2 + \tfrac{1}{3} \Delta t^2 (\sigma^2 - \gamma^2)^2 - \tfrac{1}{6} \Delta x^2 (\sigma^4 + \gamma^4) + \Delta x^2 \sigma^2 \gamma^2 + \ldots \tag{12}$$

REFLECTION OF PERIODIC WAVES FROM A SINGLE SAW-TOOTH BOUNDARY

A rigid wall is aligned at 45° to the x- and y-axes with the fluid to the left. The zero flux condition at the corresponding saw-tooth boundary reads

$$u^n_{q+s+1/2,s} = 0, \quad v^n_{q+s,s-1/2} = 0, \tag{13}$$

where $x = (q + \frac{1}{2}) \Delta x$ is the point of intersection between the boundary and the x-axis. Using equation (7) we may rewrite this conditions as

$$\frac{1}{\Delta t}(\eta^{n+1}_{q+s,s} - \eta^n_{q+s,s}) = \frac{-1}{\Delta x}(-u^{n+1}_{q+s-1/2,s} + v^{n+1}_{q+s,s+1/2}). \tag{14}$$

For interior points equation (8) is still valid. The substitution of differentiable functions $\tilde{\eta}$, $\tilde{u}$, $\tilde{v}$ into (14) combined with Taylor series expansions leads to

$$\frac{\partial \tilde{\eta}}{\partial t} = \frac{1}{\Delta x}(\tilde{u} - \tilde{v}) + \frac{1}{4}\left(-3\frac{\partial \tilde{u}}{\partial x} + \frac{\partial \tilde{u}}{\partial y} + \frac{\partial \tilde{v}}{\partial x} - 3\frac{\partial \tilde{v}}{\partial y} \right) + O(\Delta x, \Delta t). \tag{15}$$

If $\tilde{\eta}$, $\tilde{u}$ and $\tilde{v}$ satisfy the continuity equation in (1), the above equation simplifies to

$$\tilde{u}_n = \frac{\sqrt{2}}{4} \frac{\partial \tilde{u}_s}{\partial s} \Delta x + O(\Delta x^2, \Delta x \Delta t^2), \tag{16}$$

where $u_n = \sqrt{(1/2)}(v - u)$, $u_s = \sqrt{(1/2)}(u + v)$. In terms of the surface displacement the boundary condition reads

$$\frac{\partial \tilde{\eta}}{\partial n} = \frac{\sqrt{2}}{4} \frac{\partial^2 \eta}{\partial s^2} \Delta x + O(\Delta x^2, \Delta x \Delta t), \tag{17}$$

where $(\partial/\partial n) = \sqrt{(1/2)}(\partial/\partial y - \partial/\partial x)$ and $(\partial/\partial s) = \sqrt{(1/2)}(\partial/\partial y + \partial/\partial x)$; (16) and (17) demonstrate the first-order error of the saw-tooth boundary representation.

An incoming plane wave in form of a single harmonic is denoted by

$$(\eta^n_{s,p})_{\text{incom}} = A e^{i(ks\Delta x + lp\Delta x - \omega n\Delta t)}, \tag{18}$$

where k, l and ω must fit the numerical dispersion relation (9). We assume that the incoming wave will give rise only to a single reflected harmonic of the form

$$(\eta^n_{s,p})_{\text{ref}} = B e^{i(ls\Delta x + kp\Delta x - \omega n\Delta t + \delta)}. \tag{19}$$

The major difference from the analytical case is the presence of the phase shift δ. Substitution into (14) gives

$$RA + R^* e^{i\delta} B = 0, \tag{20}$$

where

$$R = \bar{\omega}^2 + \frac{1}{\Delta x^2}(e^{-ik\Delta x} + e^{il\Delta x} - 2). \tag{21}$$

A real B fitting (20) exists if

$$\delta = -\pi + 2\arg(R), \tag{22}$$

and we obtain $A = B$, which implies conservation of energy during the reflection. If $k\Delta x$, $l\Delta x$ and $\omega\Delta t$ are small, we may expand the right hand side of (22):

$$\delta \approx \frac{k^2 + l^2}{k - l}\Delta x + O(\Delta x^2). \tag{23}$$

This equation clearly illustrates the first-order accuracy of the saw-tooth boundary approximation. If $k = l$, R becomes real and we obtain $\delta = -\pi$. In this case the two harmonics cancel and we obtain no non-trivial solution. No harmonic wave may thus propagate parallel to the boundary without being influenced by its presence. We will show that the boundary instead may act as a waveguide. A wave trapped to the boundary must be of the form

$$\eta^n_{s,p} = A e^{i(\alpha(s - s_0)\Delta x + \alpha^* p\Delta x - \omega t)}, \tag{24}$$

where $\alpha = \sigma - i\gamma$ ($\gamma > 0$) and σ, γ and ω must fit the relation (11). The quantity corresponding to R in (9) has to be zero in this case, which leads to

$$0 = \bar{\omega}^2 + \frac{1}{\Delta x^2}(e^{-\gamma\nabla x}\cos(\sigma\Delta x) - 1). \tag{25}$$

We expand (25) in the same manner as (23) and obtain

$$\gamma = \tfrac{3}{4}\omega^2\Delta x + O(\Delta x^2) = \tfrac{3}{2}\sigma^2\Delta x + O(\Delta x^2). \tag{26}$$

For long waves $\sigma\Delta x \ll 1$ and the exponential decay in the normal direction to the boundary is slow. From this value of γ we obtain an e-folding distance

$$E = \frac{\lambda^2}{3\pi^2\Delta x} + O(1), \tag{27}$$

where λ is the wavelength. The boundary condition (16) is derived using the continuity equation only and will thus also be valid if the Coriolis terms are included in the equation of motion. Since γ is of order Δx the waveguide action of the boundary must be caused mainly by the discretization error of the boundary condition. The artificial trapped modes therefore still exist and may be

misinterpreted as Kelvin waves. To decide if a wave is trapped by rotational effects or not we may compare the e-folding length $E_* = hE$ to the Rossby radii $R_* = c_*/f_*$, where the asterisk indicates dimensional quantities, h is the depth, c_* equals $\sqrt{(gh)}$ and f_* is the Coriolis parameter. The rotational effects will be dominant if

$$1 \gg \frac{R_*}{E_*}. \tag{28}$$

PROPAGATION OF WAVES IN CHANNELS WITH SAW-TOOTH SHAPED LATERAL BOUNDARIES

Figure 3 shows the discretized approximation to a channel aligned at 45° to the axes. For waves propagating along such a channel, a significant decrease in phase velocity is experienced both in numerical tests and applications. This reduction of the wave speed vanishes in the limit of a infinitely wide channel. From the discussions of the previous chapter we know that no pure harmonic wave may propagate along the channel. There are two possible modifications of the wave which may account for the observed delays. First the wave may be criss-crossing along the channel in a series of reflections, as described by equations (17)–(23). Secondly the components of the wave numbers normal to the direction of the channel may be imaginary. This corresponds to trapped waves of the form (24). The natural starting point for the analysis of the phenomena is the study of the narrowest channel possible, which is depicted to the left in Figure 4.

Along this channel there is a unique path for wave propagation, which is marked by the dotted line. We rename the quantities belonging to the grid points located at this line:

$$\eta^n_{s,s} = \zeta^n_{2s}; \quad \eta^n_{s+1,s} = \zeta^n_{2s+1}; \quad u^n_{s+1/2,s} = \beta^n_{2s+1/2}; \quad v^n_{s,s-1/2} = \beta^n_{2s-1/2}. \tag{29}$$

Implementation of the boundary conditions and the new notation in equations (7) and (8) leads to

$$\frac{1}{\Delta t}(\beta^{n+1}_{s+1/2} - \beta^n_{s+1/2}) = -\frac{1}{\Delta x}(\zeta^n_{s+1} - \zeta^n_s), \quad \frac{1}{\Delta t}(\zeta^{n+1}_s - \zeta^n_s) = -\frac{1}{\Delta x}(\beta^{n+1}_{s+1/2} - \beta^{n+1}_{s-1/2}),$$

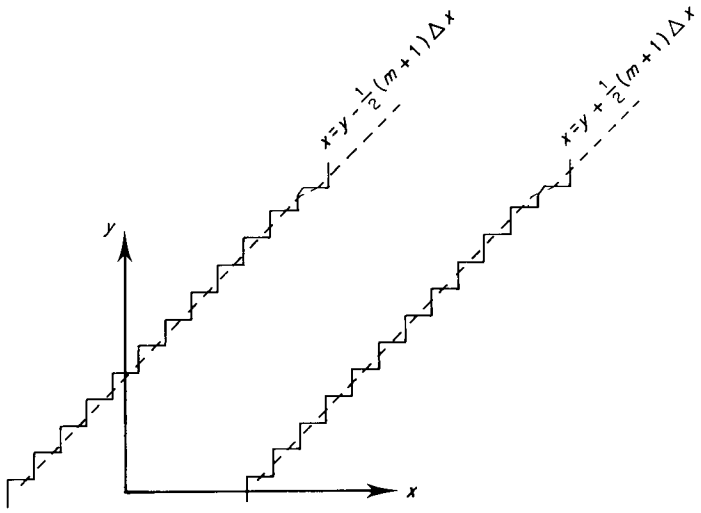

Figure 3. Definition sketch of a channel aligned at 45° to the axes

$$\frac{1}{\Delta t^2}(\zeta_s^{n+1} - 2\zeta_s^n - \zeta_s^{n-1}) = \frac{1}{\Delta x^2}(\zeta_{s+1}^n - 2\zeta_s^n + \zeta_{s-1}^n). \tag{30}$$

This set of equations is identical to the two-dimensional forms of (7) and (8). The wave speed for very long waves ($\omega\Delta t \ll 1$ etc.) will thus equal $\sqrt{(1/2)} = 0{\cdot}707\ldots$ The features of this particular case seems to support the 'criss-cross' explanation. This explanation is nevertheless wrong. On the right of Figure 4 we have drawn an imagined ray of a criss-crossing wave. The difference in phase for the right-moving wave between point (I) and point (II) is $\theta_1 - \theta_0 = \Delta\theta = k_n B + \frac{1}{2}k_s D$ where k_s and k_n are the components of the wave number parallel and normal to the channel. The phase of the left-moving wave is $\theta_2 = \theta_1 + \delta$ at (II) and $\theta_3 = \theta_2 + \Delta\theta$ at point (III). For the phase of the right moving wave at (III) we thus have two different expressions. $\theta_4 = \theta_3 + \delta = \theta_0 + 2\Delta\theta + 2\delta$ and $\theta_4 = k_s D + \theta_0$. The equality of these two expressions implies $\delta = -k_n B < 0$. Because k is larger than l for the right-moving wave (23) implies that $\delta > 0$ in the limit $k\Delta x, l\Delta x \to 0$. For long waves no criss-crossing is therefore possible and the corresponding explanation of the speed reduction must be abandoned.

Exploiting the symmetry of the channel in Figure 3 we assume the existence of a wave of the form

$$\begin{aligned}\eta_{s,p}^n &= A e^{i\sigma(s+p)\Delta x}\cosh\gamma(s-p)\\ &= \frac{A}{2}[e^{i(\alpha s\Delta x + \alpha^* p\Delta x)} + e^{i(\alpha^* s\Delta x + \alpha p\Delta x)}],\end{aligned} \tag{31}$$

where $\alpha = \sigma - i\gamma$. From (14) we obtain

$$\begin{aligned}0 &= e^{(m/2)\gamma\Delta x}(\bar{\omega}^2\Delta x^2 + e^{i\alpha^*\Delta x} + e^{-i\alpha\Delta x} - 2)\\ &\quad + e^{-(m/2)\gamma\nabla x}(\bar{\omega}^2\Delta x^2 + e^{-i\alpha^*\Delta x} + e^{i\alpha\Delta x} - 2)\\ &= e^{(m/2)\gamma\Delta x}(\bar{\omega}^2\Delta x^2 + 2e^{-\gamma\Delta x}\cos(\sigma\Delta x) - 2)\\ &\quad + e^{-(m/2)\gamma\Delta x}(\bar{\omega}^2\Delta x^2 + 2e^{\gamma\Delta x}\cos(\sigma\Delta x) = 2),\end{aligned} \tag{32}$$

where m is as defined in Figure 3. $m+1$ equals the number of η-points at the x-axis. This equation, in addition to (11), gives the dispersion relation for waves propagating along the

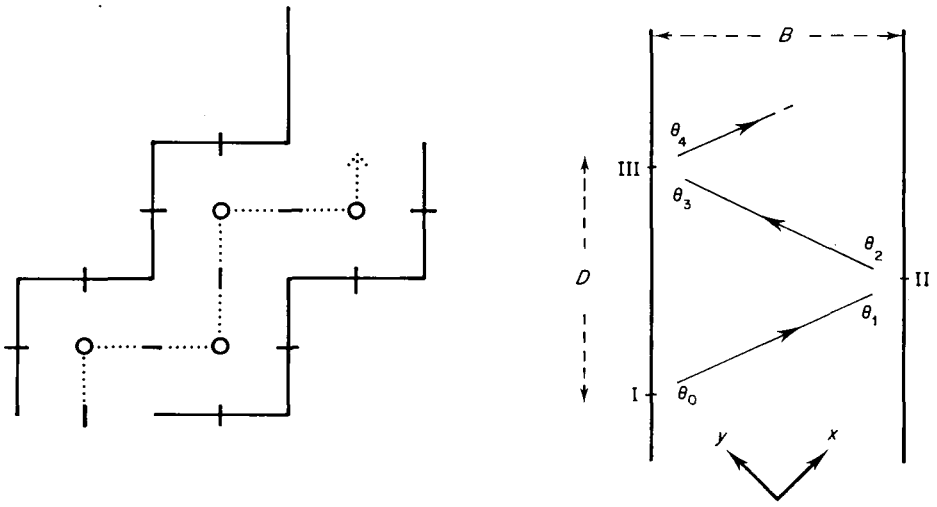

Figure 4. Left: the narrowest channel possible. Right: the path of a ray for an imagined criss-crossing wave

Table I. Wave speeds

m	c_s	Numerical experiments
1	0·7071	—
2	0·8165	0·817
3	0·8660	—
4	0·8944	0·895
6	0·9258	0·925
10	0·9535	0·954
20	0·9760	0·979

channel. Letting $\alpha\Delta x$, $\omega\Delta t \to 0$ keeping m fixed, expansion of (32) and (11) gives

$$2\sigma^2 \simeq \left(1+\frac{1}{m}\right)^2, \quad \gamma^2 \simeq \frac{1}{2m}\omega^2. \tag{33}$$

The phase speed c_s is given by

$$c_s = \frac{\omega}{k_s} = \frac{\omega}{\sigma\sqrt{2}} = \left(1+\frac{1}{m}\right)^{-1/2}, \tag{34}$$

where $k_s = \sigma\sqrt{2}$ is the component of the wave number parallel to the channel. There is a short-cut leading to equation (34). Because the numerical dispersion relation (9) is of second-order accuracy the leading discretization error stems from the modelling of the boundary. We may thus obtain (34) by solving the analytical problem defined by the combination of (2) or (5) and the boundary condition (16). Hence (34) is valid for all second-order schemes based on the present grid, having a boundary discretization error as given by (16). In Table I we have compared c_s from (34) to the speed of long single-crested pulses measured in numerical experiments by Mørk.[2] The agreement is convincing and the small discrepancies are probably due to discretization errors and inaccuracy in the wave speed measurements in the experiments.

In the limit $\alpha\Delta x$, $\omega\Delta t \to 0$ the velocity components parallel and normal to the channel are given by

$$u_s \simeq \frac{A}{c_s} e^{ik_s(x_s - c_s t)} \cosh(\sqrt{2}\gamma x_n), \tag{35}$$

$$u_n \simeq \frac{A}{\sqrt{(2m)}} e^{ik_s(x_s - c_s t)} \sinh(\sqrt{2}\gamma x_n),$$

where x_s and x_n are parallel and normal co-ordinates to the channel, respectively. In (35) we have abandoned the index notation for numerically calculated quantities. (35) illustrates that in the inner part of the channel there are no signs of any effect that may be interpreted as a no-slip condition, as observed by Weare[1] for the ADI scheme. On the contrary: u_s attains its largest values close to boundaries.

CONCLUDING REMARKS

The presence of saw-tooth shaped boundaries introduce discretization errors of first order in the grid increments. These errors may cause significant distortion and even qualitative changes of the reflection properties of the boundary. The reflections of a plane wave from such boundaries are accompanied by phase shifts and, contrary to the analytical case, there exist solutions in the

form of waves trapped to the boundary. Propagating waves in channels with lateral saw-tooth boundaries have to be of this form. Hence the component of the wave number vectors normal to the direction of the channel has to be imaginary and the phase speeds are therefore reduced. These reductions are severe for narrow channels. Even though the investigations are confined to the FB scheme the results will probably be valid for most related schemes. When discretizing a geometry, effort should be made to avoid the described effects as far as possible by choosing the appropriate orientation of the co-ordinate system.

In models including rotational effects, the artificial trapped modes described above may be confused with Kelvin waves. The influence of the saw-tooth boundary on the trapping of waves is negligible if (28) is satisfied.

REFERENCES

1. T. J. Weare, 'Errors arising from irregular boundaries in ADI solutions of the shallow-water equations', *Int. j. numer. methods eng.*, **12**, 921–931 (1974).
2. G. Mørk, 'The effect of lateral saw-tooth boundaries on the numerical phase velocity', Norwegian Hydrodynamic Laboratories, *Internal Report, project no. 609274* (1983).
3. F. Meisinger, and A. Arakawa, 'Numerical methods used in atmospheric models', WMO, *GARP Publ. Ser.*, no. 17 (1976).